[1]Oghenevwaire Akpeghagha,
Emenike C. Ejiogu,
Cajethan M. Nwosu,
Chukwudi M. Chukwudozie,
[2] Benson O. Ezea

Design and Implementation of a Modified Push-Pull Parallel-Series Resonant Converter

Abstract: - This study presents a modified Push-Pull Parallel Resonant Converter (PPRC) for efficient wireless charging of electric vehicles (EVs), addressing key limitations of the conventional Series-Series Full Bridge Resonant Converter (SS-FRC). The proposed PPRC features a dual primary coil design that integrates the resonant tank, current-splitting transformer, and DC inductor—resulting in reduced component count, simplified circuit architecture, and lower implementation cost. A scaled 18W laboratory prototype was developed to validate the design. Experimental results showed a peak efficiency of 93.4% at a 1 cm air gap, significantly outperforming the SS-FRC's 30% under the same conditions. Even at 3 cm and 5 cm gaps, the PPRC maintained superior efficiency. The converter also demonstrated improved soft-switching behavior, reduced voltage spikes, and enhanced waveform stability. Compared to existing push-pull and cascaded designs in literature, the PPRC offers comparable or better performance with less complexity. Additionally, the system incurs approximately 50% less conduction loss than the SS-FRC and operates at the SAE J2954 standard frequency of 85 kHz, making it suitable for current-generation wireless EV charging infrastructure. This work contributes a practical, cost-effective solution for next-generation inductive power transfer systems and offers valuable insights into converter topology design and energy optimization for smart EV charging.

Keywords: Wireless Power Transfer (WPT), Electric Vehicle Charging, Push-Pull Resonant Converter, Inductive Power Transfer (IPT), Converter Efficiency Optimization.

I. INTRODUCTION

Wireless Power Transfer (WPT) has emerged as a promising technology for enhancing the convenience safety, and automation of electric vehicle (EV) charging systems. Among various WPT techniques, Inductive Power Transfer (IPT) is widely adopted due to its efficiency and suitability for high-power applications. Central to IPT systems is the inverter topology that drives the primary coil, and the current-fed push-pull parallel resonant inverter (CFPPRI) has shown potential due to its current-limiting behavior, simplified control, and soft-switching capability under resonance conditions. The traditional Series-Series Full Bridge Resonant Converter (SS-FRC), while commonly used, suffers from limitations such as high conduction losses, sensitivity to air gap variations, and complex switching requirements. To address these challenges, several researchers have proposed variations of the push-pull topology. In [1], a modified CFPPRI incorporating diodes in series with switches achieved reduced total harmonic distortion (THD), though it introduced diode voltage drop losses and did not meet standard WPT frequency requirements. Another study in [2] employed a Cascaded Class D inverter to minimize switch voltage stress, yielding high efficiency but resulting in a bulky and complex design. Adaptive tuning methods using PWM-controlled resonant tanks [3] improved soft switching but significantly increased circuit complexity and component count. Similarly, the Symmetrical Half-Bridge Resonant Converter (SHRC) proposed in [4] demonstrated reduced losses but operated at low frequencies (12.5 kHz), far below the SAE J2954-recommended 85 kHz for EV wireless charging. These approaches, while beneficial in certain respects, reveal a persistent trade-off between efficiency and circuit simplicity. Most do not fully resolve the need for a compact, cost-effective, and highly efficient solution that performs well under variable load and misalignment conditions

In this study, a modified Push-Pull Parallel Resonant Converter (PPRC) featuring a dual primary coil configuration that serves concurrently as a DC inductor, phase-splitting transformer, and resonant tank is introduced. This integration significantly reduces the converter's size and component count while enhancing magnetic coupling and energy transfer efficiency. The topology also ensures better soft-switching performance and reduced voltage stress without requiring complex tuning networks or additional auxiliary circuits. To validate the design, a scaled 18W laboratory prototype was developed and benchmarked against the conventional SS-FRC. This work contributes a practical, scalable solution that addresses current design challenges in WPT systems for EVs, offering an optimal balance of efficiency, simplicity, and cost-effectiveness for real-world implementation.

[1] *Corresponding author: Department of Electronic and Computer Engineering, University of Nigeria, Nsukka.
Africa Centre of Excellence for Sustainable Power and Energy Development
University of Nigeria, Nsukka. chukwudi.chukwudozie@unn.edu.ng
[2] Bowling Green State University

II. MATERIAL AND METHODS

Computational Modeling of H-Bridge Series-Series Compensation Topology

The following equation gives an expression for the coupling coefficient k:

$$k = \frac{M}{\sqrt{L_P L_S}}, \quad (1)$$

the inductance of the Tx coil is denoted as L_P while the inductance of the Rx coil is denoted as L_S. M represents the mutual inductance. A capacitor correction is used to offset the weakly coupled inductive coils' leakage inductance. Nonetheless, the functions of the compensation utilized in the primary and secondary sides of the circuitry differ. The compensation capacitance at the primary side C_P and that of the secondary side C_S of the WCS is computed at resonance using the frequency ω as shown in equation (2) [5]–[8]

$$\omega = \frac{1}{\sqrt{L_P C_P}} = \frac{1}{\sqrt{L_S C_S}} \quad (2)$$

The resonance frequency is denoted by ω and it is measured in rad/sec.

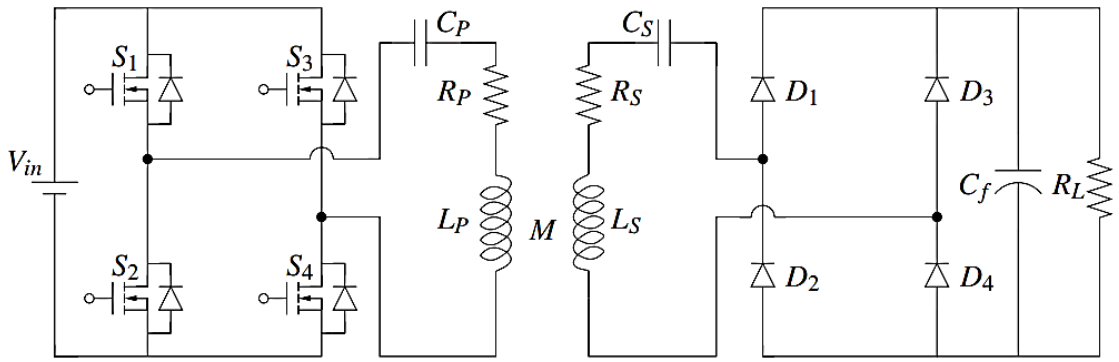

Figure-1. Series-Series compensation for a WEVCS

Figure 1 illustrates the circuit of the wireless charging system using the Series-Series compensation. The H-bridge inverter is used to realize a high frequency pulsating DC. The output of the H-bridge inverter is sent to the primary compensated coil. To achieve a DC voltage at the receiver side of the WEVCS, a diode bridge rectifier is utilized. The primary coil's winding resistance is represented by the letter R_P, while that of the secondary coil is depicted by the letter R_S. The WEVCS uses a high frequency H-bridge inverter. This inverter's fundamental function is dependent on the switching of power semiconductor devices. A diode bridge rectifier is utilized on the receiver circuit for recharging the battery.

Using Figure 1, the magnitude of the impedance at primary section of the circuit Z_P and the secondary section of the circuit Z_S for the h^{th} harmonic are determined; the formulas are shown in Equations (3) and (4) [9].

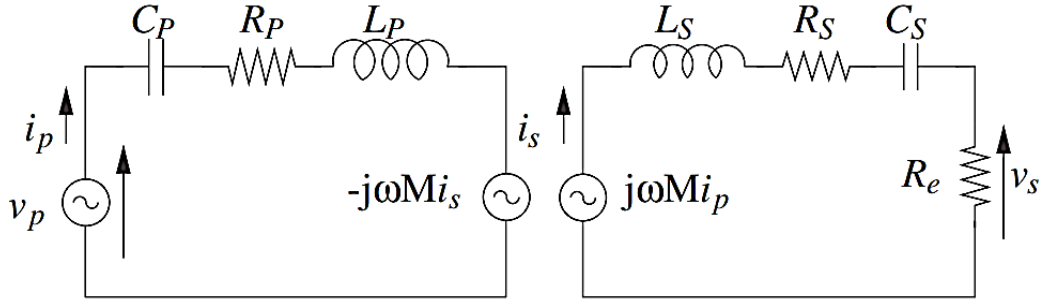

Figure-2. Equivalent circuit model of series-series compensation for WEVCS.

$$Z_P = R_P + j\left(h\omega L_P - \frac{1}{h\omega C_P}\right) \quad (3)$$

At the receiver side of the WCS, the voltage source is realized through induction. The impedance at the receiver side circuitry is expressed by (4):

$$Z_S = R_S + R_e + j\left(h\omega L_S - \frac{1}{h\omega C_S}\right) \quad (4)$$

where R_e represents the effective load resistance.

$$R_e = \frac{8}{\pi^2} R_L \quad (5)$$

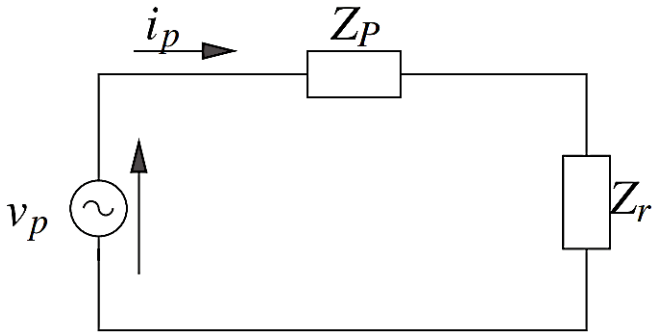

Figure-3. Equivalent impedance at the receiver side of the WEVCS circuit.

With reference to the transmitting side of the WEVCS circuit, the impedance at the receiver side, Z_S (see Figure 3) is expressed mathematically as shown in Equation (6).

$$Z_S = \frac{(h\omega M)^2}{R_S+R_e+j\left(h\omega L_S-\frac{1}{h\omega C_S}\right)} \tag{6}$$

Hence, total impedance,

$$Z_T = R_P + j\left(h\omega L_P - \frac{1}{h\omega C_P}\right) + \frac{(h\omega M)^2}{R_S+R_e+j\left(h\omega L_S-\frac{1}{h\omega C_S}\right)} \tag{7}$$

Since the internal resistance of a coil is far larger than the parasitic resistance of inductors and capacitors, they may be disregarded. The most fundamental resonance structure is the SS topology. Series resonance is used by both the transmitter and receiver side. Figure 4 depicts the analogous circuit, where M signifies the mutual inductance and U_s is a steady voltage stabilized.

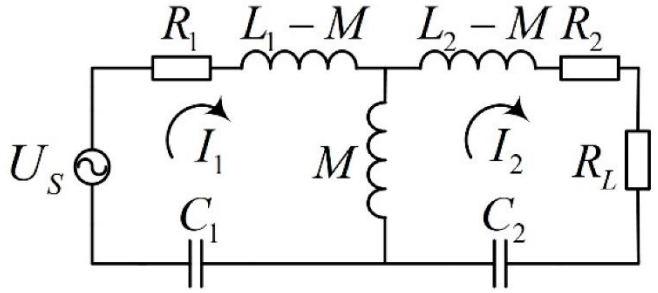

Figure-4. Fundamental model of the SS-topology

With the of Kirchhoff voltage law (KVL), the above circuit can be further simplified as [10]:

$$\begin{cases} \left(R_1 + j\omega L_1 + \frac{1}{j\omega C_1}\right) I_1 - j\omega M I_2 = U_s \\ \left(R_2 + R_L + j\omega L_2 + \frac{1}{j\omega C_2}\right) I_2 - j\omega M I_1 = 0 \end{cases} \tag{8}$$

At resonance:

$$f_0 = \frac{1}{2\pi\sqrt{L_1 C_1}} = \frac{1}{2\pi\sqrt{L_2 C_2}} \tag{9}$$

When $R_L >> R_1$ and R_2, R_1 and R_2 can be disregarded, the currents I_1 and I_2 is realized as:

$$\begin{cases} I_1 = \frac{U_S R_L}{(\omega M)^2} \\ I_2 = \frac{U_S}{\omega M} \end{cases} \tag{10}$$

The transmission power is given by:

$$P_{ss} = \frac{U_S^2 R_L}{(\omega M)^2} \tag{11}$$

Also, the system efficiency is computed mathematically as:

$$\eta_{ss} = 1 - \frac{R_L R_1}{(\omega M)^2} - \frac{R_2}{R_L} \tag{12}$$

When load value is taken into consideration, the maximum efficiency that could be realized is given as:

$$\eta_{ss\_max} = 1 - \frac{2\sqrt{R_1 R_2}}{\omega M} \tag{13}$$

In real-world applications, it is typical for the receiver coil to be located at a distance from the transmitter coil because of the inverted connection between distance and mutual inductance. From Equations (10) and (11), it is evident that the transmitter current will grow dramatically while the receiver side is open, and that the transmitter current and transmission power will drop when there is a short circuit on the receiver side. Conversely,

for the SS construction with fixed coil characteristics, the load resistance must remain constant to get maximum efficiency.

Proposed Optimal Compact Push-Pull Parallel-Series Resonant Converter

As outlined in [2], the push-pull resonant inverter faces the limitation of requiring a gate driving circuit to achieve zero-voltage switching (ZVS). This introduces a challenge due to the necessity for initial energy. To address this issue, it is crucial to ensure that some energy is present in the circuit during the start-up phase. One approach to achieve this is by employing a polyphase strategy to guarantee energy availability during initialization, as detailed. This method involves standardizing the coupling between phases [11]. Alternatively, integrating the advantages of the Cascaded Class D inverter (which mitigates voltage stress) a common issue with current-fed converters with the benefits of the push-pull resonant inverter can provide a solution. This combined approach is illustrated in [2].

In real-world applications, the output of a traditional CFPPRI often exhibits distortion when operating off-resonance. To mitigate the issues caused by frequency deviation, one approach involves dynamically tuning the switching frequency to match the system's resonant frequency [12]. An alternative method is to incorporate a diode in series with each switch to address the mismatch-related challenges as discussed in [1], [13]. In this study an ultra-fast switching diode is utilized to make one of the switches unidirectional in order to achieve ZVS and steady resonance operation.

A compact push-pull current-fed hybrid resonant converter that combines two primary coil configurations with all magnetic components is proposed in this study. Figure 5 shows the suggested resonant converter. The Wireless Charging System's primary coil and secondary coil is made up of inductor L_p *and* L_s respectively. Three key potentials of the proposed compact design provided by this combination primary coil include:

i. Serves as the DC inductor required for the operation of a current-fed resonant converter.
ii. Splits the DC current by acting as a phase-splitting transformer.
iii. Acts as an LC oscillation resonant circuit.

Depending on which way each coil is wound, there can be a positive or negative coupling between L_p *and* L_s. Keep in mind that two coils with a negative coupling coefficient have a 180-degree phase difference despite being positively coupled. Loosely linked inductors are equal to a completely coupled phase-split transformer having a shared DC inductor.

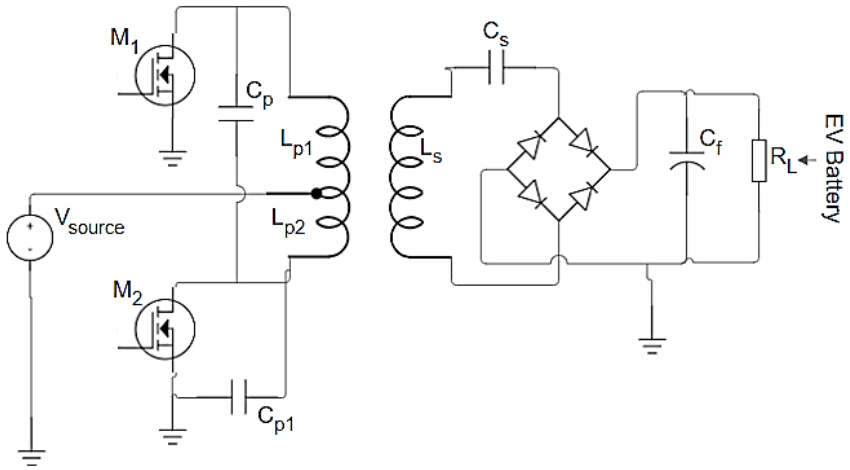

Figure-5. Schematic Proposed Compact Push-Pull Parallel-Series Resonant Converter

The following is a representation of the phase-splitting transformer of the primary winding and its corresponding DC inductor:

$$L_1 = \frac{(L_a - kL_b)}{2} \quad (14)$$

$$L_p = \frac{(L_a + kL_b)}{2} \quad (15)$$

Where L_1 represents the equivalent DC inductor, L_a *and* L_b are the respective inductances of the phase splitting transformer primary coils and L_p represents the value of the resultant of each of the split coils at the primary. Coupling coefficient, K, is expressed as:

$$K = M\sqrt{L_a L_b} \quad (16)$$

In this context, M characterizes the mutual inductance linking the primary coils.

The combined inductors in the suggested compact converter make it more difficult to analyze how each inductor affects the behavior of the converter as a whole. The converter coil current cannot be considered to be sinusoidal any longer. A straightforward second order linearized state space model is unable to predict the circuit operation under these circumstances. Therefore, a stroboscopic mapping model, a more complex analytical study, is needed [14]. The system can be classified into two phases as a result of the switching operation:

Phase 1: M1 is HIGH and M2 is LOW.

Phase 2: M2 is HIGH and M1 is LOW.

It is important to highlight that, except when the switching frequency (fs) exactly matches the resonant frequency (fr), the power transistors are activated while a non-zero voltage is present across them—indicating operation under hard-switching conditions. Nevertheless, the resulting switching losses are significantly lower than those encountered in the off-resonant operation of a conventional push-pull parallel resonant converter, where the transistors effectively short-circuit the resonant capacitor. Given the previously described functionality of the proposed push-pull parallel resonant topology—and acknowledging that only one switch conducts per half-cycle—the converter's behavior can be effectively represented by a parallel resonant circuit driven by a square-wave current source.

The harmonic characteristic of the equivalent current source is represented as[1]:

$$I(t) = \frac{4I_{DC}}{\pi}\sum_{k=0}^{\infty}\frac{1}{2k+1}\sin(2k+1)\omega_r t \quad (17)$$

$$\omega_r = 2\pi f_r \quad (18)$$

The DC current of the input inductor L_1 is given by I_{DC}, the frequency of resonance is denoted by ω_r and the index value of the harmonic stages is represented by k.

Therefore, the impedance of the resonant network can be expressed as:

$$Z(s) = \frac{S\omega_r}{S^2+S\frac{\omega_r}{Q}+{\omega_r}^2} \quad (19)$$

'S' represents the Laplace operator. Also, the quality factor, Q, is expressed as:

$$Q = \frac{R_L}{Z_r} \quad (20)$$

R_L represents the load resistance and the resonant network impedance is denoted as Z_r, mathematically written as:

$$Z_r = \sqrt{\frac{L_p}{C_p}} = \sqrt{\frac{L_s}{C_s}} \quad (21)$$

Under steady state scenario,

$$S = jk\omega_r, \quad (22)$$

The absolute value of the network impedance corresponding to a specific harmonic is expressed in its normalized form:

$$|Z(k\Omega)| = \left|\frac{jk\omega_r}{Z_r}\right| = \frac{1}{\sqrt{\frac{1}{Q^2+\left(k\Omega-\frac{1}{k\Omega}\right)^2}}} \quad (23)$$

Where Ω represents the ratio between the frequency of resonant (ω) and the operating or running frequency (ω_r):

$$\Omega = \frac{\omega}{\omega_r} \quad (24)$$

The k^{th} harmonic of the voltage at the output is defined by:

$$V_{out}(k) = I_k \cdot Z_k \quad (25)$$

the rms for the voltage at the output is expressed as:

$$V_{out\_rms} = \sqrt{\sum_{k=0}^{\infty}\frac{V_{out}(k)^2}{2}} \quad (26)$$

When discussing circuits designed to enhance switching speed, the primary focus often falls on circuits that accelerate the turn-off process of MOSFETs. This is important to note since the rectifier component in the power supply's turn-off or reverse recovery time usually limits the turn-on speed. As such, the greatest switching speed that may be achieved depends more on the reverse recovery properties of the diode than on the gate drive circuit's capacity. The switching properties of the diode are synced with the gate drive speed at turn-on in an ideal setup. A greater voltage can be placed across the driver output impedance and gate resistor since the Miller region is closer to ground than the final gate drive voltage (V_{DRV}). This usually results in a sufficient turn-on speed for the MOSFET.

When the switch is off, the situation is very different. The gate drive circuit is the only component that theoretically influences the MOSFET's turn-off speed. The input capacitors can be discharged more quickly via a more reliable turn-off circuit, which reduces switching losses and shortens switching times. Using a MOSFET driver with a lower output impedance or, in the case of N-channel devices, using a negative turn-off voltage can help achieve greater discharge currents. The larger di/dt and dv/dt of the MOSFET in turn-off speed-up circuits can cause more ringing in the waveforms, even if enhanced switching speed can reduce switching losses. When

choosing suitable voltage ratings and EMI mitigation techniques for the power device, this effect should be taken into account.

An anti-parallel diode can be added to increase the turn-off speed in a straightforward manner, as illustrated in Figure 6.

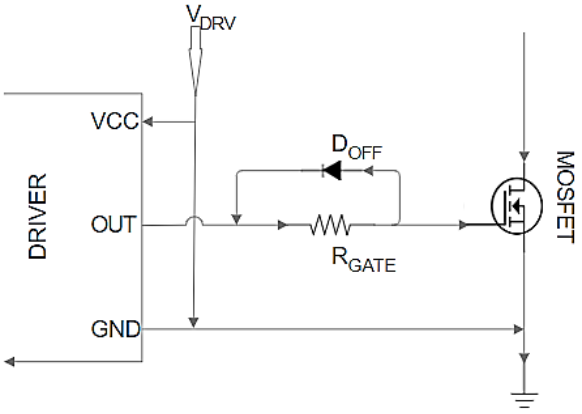

Figure-6. Circuit for Enhancing the Turn-Off Speed Using an Anti-Parallel Diode

In this circuit, R_{GATE} is used to control the turn-on speed of the MOSFET. When turning off, the antiparallel diode effectively bypasses the resistor. The, D_{OFF} component is active only when the gate current surpasses the threshold defined in Equation (27).

$$I_G > \frac{V_{D,FWD}}{R_{GATE}} \quad (27)$$

The 1N4148 diode, gives a gate current of approximately 150 mA, and when utilizing a BAS40 Schottky antiparallel diode, it is approximately 300 mA. As the gate-to-source voltage nears 0 V, the diode's effectiveness diminishes progressively. Consequently, while this circuit significantly reduces turn-off delay time, it offers only marginal improvements in overall switching times and $^{dv}/_{dt}$ tolerance.

Circuit Design in Proteus

The proposed optimal configuration of the push pull and the conventional Series-series resonant H-bridge inductive charging circuit were designed using the Proteus simulation software. This was done to gain insight into the waveform of the current and voltage generated at the transmitter side of the circuitry and as well test run the design parameters before implementing a prototype. Figure 7 and Figure 8 shows the circuitry designed in Proteus. Results from this simulation are presented and discussed in the following chapter.

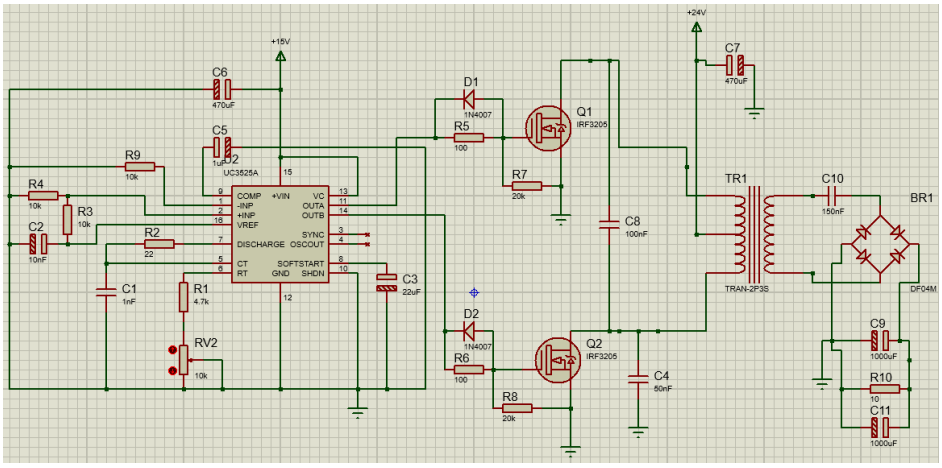

Figure-7. Design of the proposed Push-Pull resonant converter in Proteus

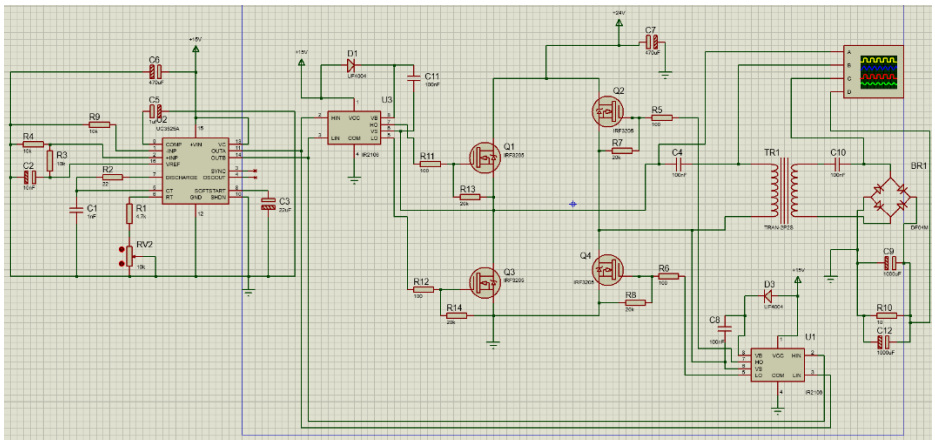

Figure-8. Series-series resonant H-bridge converter design in Proteus

Design Specifications for Laboratory Prototype Implementation

Table 1 gives some key design parameters/components used for the implementation of the proposed circuitry as well the conventional series-series H-bridge circuitry. The inductances of the primary and secondary were specifically measured using an LCR meter.

Table-1. Design Specifications

S/N	Parameter/ Components	Proposed PPRC	SS H-Bridge
1	Mosfets	Hy1906	Hy1906
2	Diodes	IN4148, UF4007	IN4148, UF4007
3	Cp (Film Capacitors)	Cp1-100nF, Cp2-50nF	34nF
4	Cs (Film Capacitors)	150	150nF
5	Lp (14 SWG Copper wire)	Center tapped Lp1~24uH [5 turns, diameter= 40cm]; Lp2~31.7uH [(5½ turns, diameter= 40cm]	~103.44uH (11½ turns, diameter= 40cm)
6	Ls (14 SWG Copper wire)	~24uH (5 turns, diameter= 40cm)	~24uH (5 turns, diameter= 40cm)
7	R_L (Cement ceramic power resistor)	3.3Ω (30Watts)	3.3Ω (30Watts)

Laboratory Prototype Setup

Figure 9 shows the laboratory prototype setup used for experimenting the designed circuitry simulated and discussed in this study. The results from this setup are presented and discussed in the following chapter.

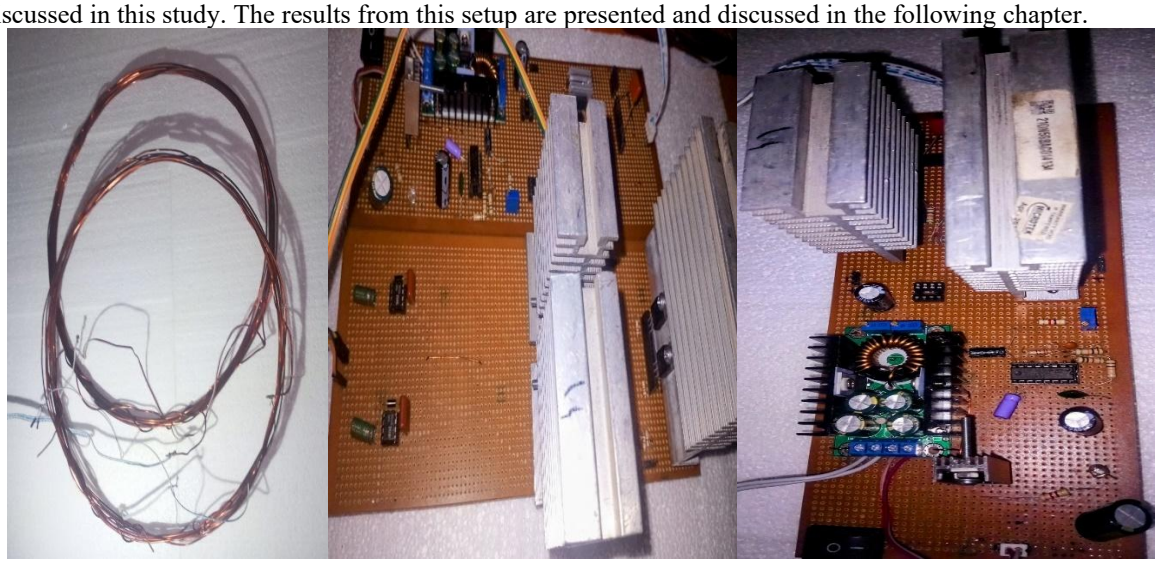

(a) (b) (c)

Figure-9. Setup of Laboratory Prototype (a) Tx and Rx Coils (b) FRC (c) proposed PPRC

III. RESULTS AND DISCUSSIONS

In order to demonstrate the potentials of the proposed inductive resonant circuitry the conventional H-bridge converter design approach has been designed for the purpose of comparison and validation. The parameters examined include the output waveforms of the transmitter side circuitry, dynamics of each circuitry under load variation, power transfer efficiency, voltage gain and misalignment tolerance. The battery of an EV can be seen as a capacitive load, hence, this was considered in modeling the load resistance in this investigation. The circuits were energized using a 24V DC source.

Experimental Results from Laboratory Prototype Setup

With the aid of an Oscilloscope the waveforms of the designed circuitry were effectively seen and the performance of the proposed push-pull and conventional SS H-bridge converter circuitry was properly studied after implementation. The output waveform of the SG3535 is shown in Figure 10.

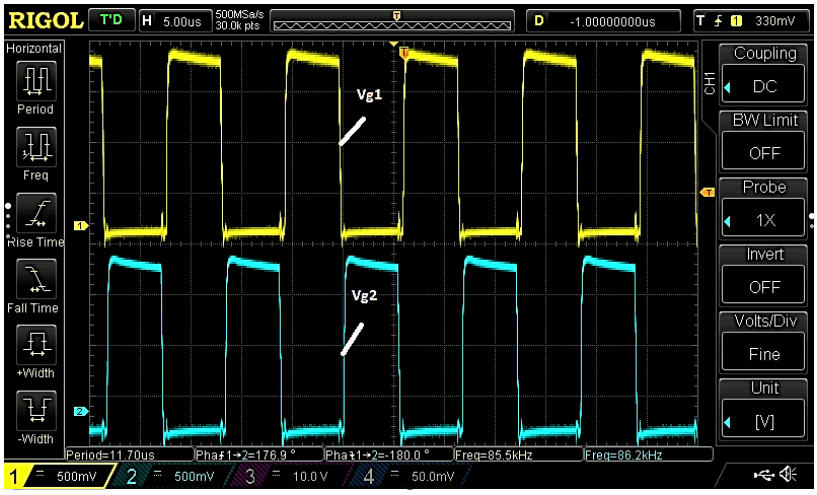

Figure-10. PWM gate signals generated from SG3525

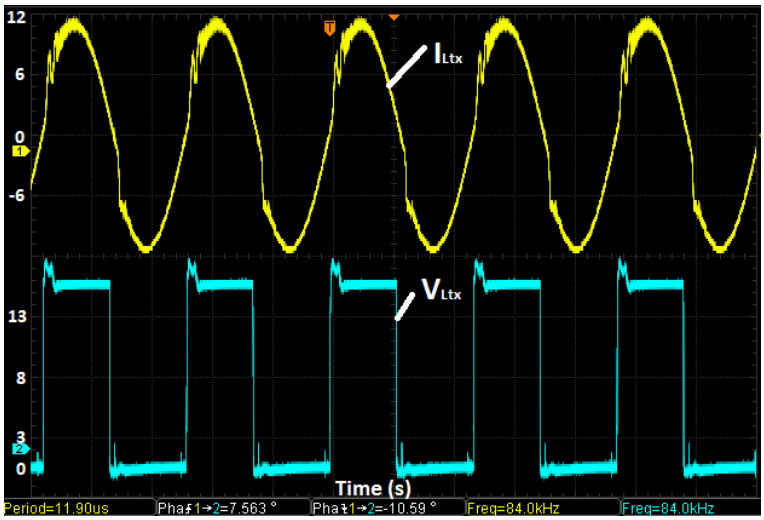

Figure-11. Current and voltage waveforms for SS-FRC

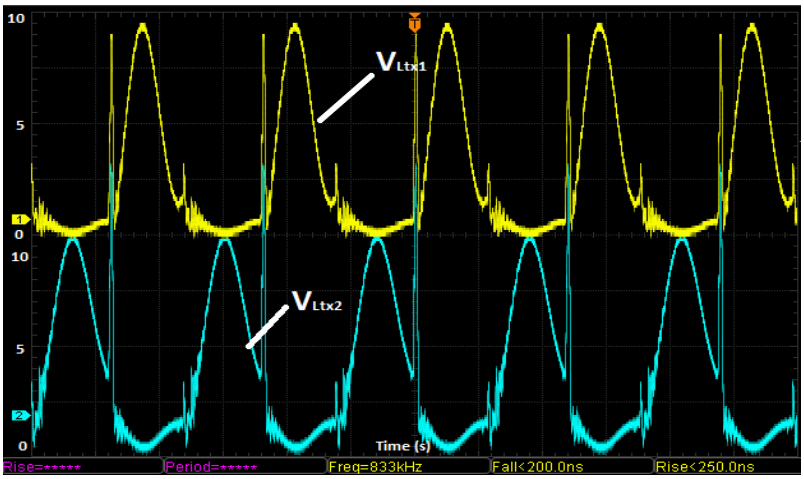

Figure-12. Current and voltage waveforms of conventional PPRC

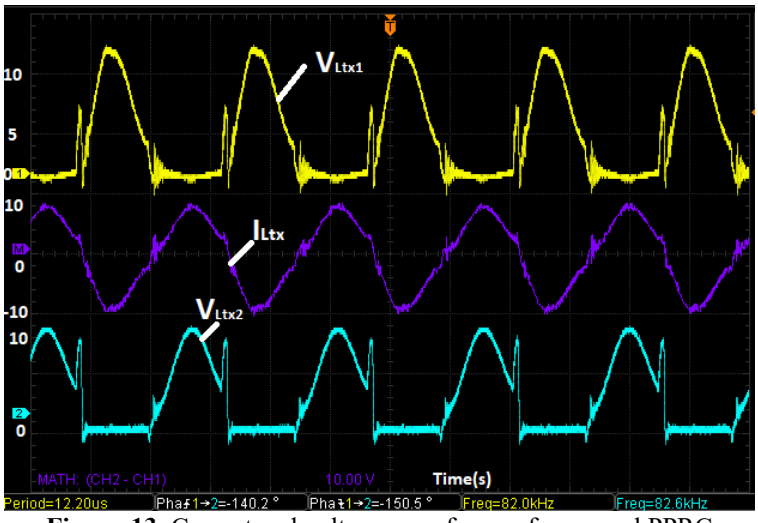

Figure-13. Current and voltage waveforms of proposed PPRC

The laboratory hardware prototype design allows for a comprehensive evaluation of the output waveforms obtained from both the conventional series-series full-bridge resonant converter and the modified push-pull resonant converter. The experimental results provide insights into the operational efficiency and performance characteristics of each converter topology in a real-world scenario.

As illustrated in **Figure 10**, the PWM gate signals generated by the SG3525 showcase two square waveforms that are phase-shifted by 180 degrees. This phase shift is essential for the effective operation of both the conventional

and modified resonant converters, ensuring that the switches operate in a complementary manner. The precise timing of these signals plays a crucial role in the overall performance, influencing the resonant behavior and efficiency of the energy transfer.

The output waveform of the series-series full bridge resonant converter is depicted in **Figure 11**. Here, a sinusoidal current waveform is observed at the transmitter coil, which indicates efficient energy transfer during operation. This waveform signifies that the current is following a resonant profile, which is a desired characteristic in resonant converters as it facilitates effective power delivery.

However, the voltage waveform across the transmitter coil appears as a square waveform, reflecting the on-off switching nature of the full bridge configuration. While this square waveform effectively drives the coil, it can also introduce harmonics and losses due to the sharp transitions between on and off states. The presence of these harmonic components may lead to additional heating and reduced overall efficiency.

In **Figure 12**, the output voltage waveform for both coils of the transmitter in the centre-tapped conventional push-pull resonant converter is shown. This waveform exhibits a half-wave sinusoidal shape, which is indicative of the converter's operation. However, noticeable spikes appear at the transition points when one switch turns off, and the other turns on. These spikes result from the tank voltage not being fully discharged before the switching action occurs, leading to voltage overshoot. This behavior highlights the limitations of the conventional push-pull resonant converter, particularly in terms of voltage regulation and energy efficiency. Such spikes can introduce stress on the components and potentially impact the longevity and reliability of the system.

Figure 13 presents the voltage and current waveforms for the modified push-pull resonant converter. The output waveforms show improved switching operations compared to the conventional design. While a minor spike can be observed at the turn-off of one of the switches, it is significantly less pronounced than in the conventional push-pull converter. Importantly, this spike does not affect the smooth operation of the resonance circuit, nor does it lead to any shifts in the resonant frequency. This indicates a more stable performance, which is a critical advantage in maintaining the efficiency and effectiveness of the wireless charging system.

Moreover, the modified push-pull resonant converter demonstrates the capability to be tuned to resonate at the same frequency as the switching frequency. This feature allows for optimal performance under varying load conditions, enhancing the overall efficiency of energy transfer. The sinusoidal current waveform observed in the proposed push-pull resonant converter design further illustrates its capability to provide efficient power delivery, minimizing losses and improving overall system reliability.

The comparative analysis of the output waveforms from both the conventional series-series full bridge resonant converter and the modified push-pull resonant converter reveals significant insights into their operational characteristics. The modified push-pull resonant converter exhibits distinct advantages, including improved switching performance, reduced voltage spikes, and enhanced tuning capabilities, leading to more efficient and reliable operation for wireless charging applications in electric vehicles. These findings underscore the potential of the modified design to optimize the performance of wireless power transfer systems, paving the way for advancements in EV charging technologies.

Evaluation of Proposed System Design

From the experimental setup the power efficiency was evaluated for an air gap distance of 10mm, 30mm and 50mm for both the conventional S-S H-Bridge setup and the proposed Push-Pull experimental setup. Table 2 below gives details of the obtained results.

Table-2. Global Efficiency Evaluation for the modified PPRC and the Conventional SS-FRC

Converter Topology	V_{in} (V)	I_{in} (A)	R_e (Ω)	P_{in} (W)	*1cm Airgap Distance*			*3cm Airgap Distance*			*5cm Airgap Distance*		
					V_{out} (V)	P_{out} (W)	Efficiency (η)	V_{out} (V)	P_{out} (W)	Efficiency (η)	V_{out} (V)	P_{out} (W)	Efficiency (η)
SS-FRC	18	1	2.67	18	3.2	3.8	30%	4.5	7.6	42.1%	5.4	11	61%
Modified PPRC	18	1	2.67	18	6.7	16.8	93.4%	6	13.5	75%	5	9.4	52%

Table 2 presents a clear comparative performance analysis of the two converter topologies under different air gap conditions: 10 mm (1 cm), 30 mm (3 cm), and 50 mm (5 cm). These measurements provide a realistic

representation of practical deployment scenarios in wireless electric vehicle charging systems (WEVCS). The efficiency results from Table 2 are as follows:

Table-3. Efficiency Results

Air Gap	SS-FRC Efficiency	Modified PPRC Efficiency
1 cm	30%	93.4%
3 cm	42.1%	75%
5 cm	61%	52%

From these observations, several key insights emerge:

1. Superior Near-Field Performance of PPRC: The modified PPRC achieved 93.4% efficiency at a 1 cm air gap, which is significantly higher than the SS-FRC's 30%. This indicates the PPRC is optimized for applications where transmitter (Tx) and receiver (Rx) coils can be aligned with minimal vertical separation—ideal for robotic EV charging stations or guided parking systems.
2. Efficiency Degradation with Distance: Both systems showed declining efficiency as the air gap increased, which is expected due to reduced magnetic coupling. However, the PPRC's efficiency reduced more sharply than the SS-FRC, suggesting its effectiveness is highly sensitive to spatial alignment and proximity.
3. SS-FRC Favorability at Fixed Gaps: At a 5 cm air gap, the SS-FRC achieved its highest efficiency (61%), surpassing the modified PPRC (52%). This suggests that the SS-FRC's design is more robust for longer-range power transfer, which may be more appropriate in loosely coupled, variable-distance scenarios.

These findings imply that converter topology selection should be application-specific:
For Controlled Environments (e.g., autonomous garages or EV fleets using robotic arms), where alignment and small air gaps can be guaranteed, the PPRC offers clear advantages. Its high efficiency minimizes energy losses, shortens charging times, and reduces thermal stress on components.
For General Public Charging Stations, where EVs may not always be precisely parked and air gaps are variable, the SS-FRC remains more practical. Despite its lower near-field efficiency, it demonstrates greater tolerance to increased distances, offering more stable and predictable performance.

ACKNOWLEDGEMENT
The authors wish to thank the Africa Centre of Excellence for Sustainable Power and Energy Development (ACESPED), University of Nigeria for its support.

CONCLUSION

This thesis presented the design, simulation, prototyping, and performance evaluation of an energy-optimized wireless electric vehicle charging system using a modified Push-Pull Parallel Resonant Converter (PPRC). The research addressed critical limitations inherent in the conventional Series-Series Full Bridge Resonant Converter (SS-FRC), including lower efficiency at small air gap distances, high component stress due to voltage spikes, and poor adaptability to dynamic charging conditions.
Through analytical modeling, circuit simulation using Proteus, and physical laboratory experiments, the proposed PPRC demonstrated remarkable performance improvements. Specifically, the PPRC achieved a global efficiency of up to 93.4% at a 1 cm air gap, significantly outperforming the SS-FRC under the same conditions. The experimental results validated the theoretical predictions, confirming the PPRC's superior soft-switching behavior, reduced voltage overshoot, and enhanced power transfer efficiency at close coupling distances.
While the SS-FRC showed better performance at wider air gaps (e.g., 61% at 5 cm), the modified PPRC exhibited unmatched efficiency in controlled environments where alignment and coil proximity can be managed—making it highly suitable for autonomous EV charging stations and smart robotic applications. The PPRC's compact design, lower conduction losses, and improved waveform quality further enhance its practical value and application potential in modern EV infrastructure.
In addition, the efficiency analysis underscored the critical role of converter topology, coil design, and system resonance tuning in optimizing wireless power transfer. This work also contributed to expanding the practical understanding of high-frequency inverter losses, air-gap sensitivity, and the impact of parasitic elements on system behavior. Further optimization can be made in the following areas:

1. **Hybrid Approaches**: An interesting research direction could involve hybrid converter topologies that can adaptively switch between SS-FRC and PPRC modes based on coil alignment, load demand, or air gap measurements.
2. **Smart Alignment Systems**: Integrating sensors for real-time coil alignment, or designing self-adjusting coil mounts, can help maintain optimal gap conditions, thus ensuring that the PPRC always operates near its peak efficiency.
3. **Dynamic Compensation Networks**: To further enhance misalignment tolerance, integrating adaptive or tunable compensation networks with the PPRC topology could reduce performance dips at larger gaps.

REFERENCES

[1] M. M. Peretz and S. Ben-Yaakov, "Analysis of the Current-Fed Push-Pull Parallel Resonant Inverter Implemented with Unidirectional Switches," in *IEEE 36th Conference on Power Electronics Specialists, 2005.*, 2005, pp. 880–884.

[2] A. A. A. Abdelaziz, "Wireless Power Transfer Methods," *Politec. Milano*, 2022.

[3] S. Ali Khan and D. Ahn, "Automatic Resonance Tuning With ON/OFF Soft Switching for Push–Pull Parallel-Resonant Inverter in Wireless Power Transfer," *IEEE Trans. Power Electron.*, vol. 37, no. 9, pp. 10133–10138, Sep. 2022.

[4] J. Hong, M. Guan, Z. Lin, Q. Fang, W. Wu, and W. Chen, "Series-Series/Series Compensated Inductive Power Transmission System with Symmetrical Half-Bridge Resonant Converter: Design, Analysis, and Experimental Assessment," *Energies*, vol. 12, no. 12, p. 2268, Jun. 2019.

[5] Adebayo, M. Deepfakes and Data Privacy: Navigating The Risks in the Age of AI. NDPC–, 106.

[6] K. Aditya and S. S. Williamson, "Comparative study of Series-Series and Series-Parallel compensation topologies for electric vehicle charging," in *2014 IEEE 23rd International Symposium on Industrial Electronics (ISIE)*, 2014, pp. 426–430.

[7] K. Aditya and S. S. Williamson, "Comparative study of series-series and series-parallel topology for long track EV charging application," in *2014 IEEE Transportation Electrification Conference and Expo (ITEC)*, 2014, pp. 1–5.

[8] J. Bing, J. Wang, L. Chen, W. Bin, and Q. Wang, "A efficient control method for series-parallel CPT system," in *Proceedings of the 33rd Chinese Control Conference*, 2014, pp. 3500–3504.

[9] E. R. Joy, B. K. Kushwaha, G. Rituraj, and P. Kumar, "Analysis and comparison of four compensation topologies of contactless power transfer system," in *2015 4th International Conference on Electric Power and Energy Conversion Systems (EPECS)*, 2015, pp. 1–6.

[10] B. K. Kushwaha, G. Rituraj, and P. Kumar, "Mathematical model of series-series compensation for contactless power transfer system," in *IECON 2015 - 41st Annual Conference of the IEEE Industrial Electronics Society*, 2015, pp. 001321–001326.

[11] F. Wen, X. Chu, Q. Li, and W. Gu, "Compensation Parameters Optimization of Wireless Power Transfer for Electric Vehicles," *Electronics*, vol. 9, no. 5, p. 789, May 2020.

[12] A. Abdolkhani, A. P. Hu, and J. Tian, "Autonomous Polyphase Current-Fed Push–Pull Resonant Converter Based on Ring Coupled Oscillators," *IEEE J. Emerg. Sel. Top. Power Electron.*, vol. 3, no. 2, pp. 568–576, Jun. 2015.

[13] S. S. Ben-yaakov and M. M. Peretz, "A Self-Adjusting Sinusoidal Power Source Suitable for Driving Capacitive Loads," *IEEE Trans. POWER Electron.*, vol. 21, no. 4, pp. 890–898, 2006.

[14] J. M. Alonso, J. Cardesin, J. A. Martin-Ramos, J. Garcia, and M. Rico-Secades, "Using Current-Fed Parallel-Resonant Inverters for Electro-Discharge Applications : A Case of Study," *Ninet. Annu. IEEE Appl. Power Electron. Conf. Expo.*, vol. 1, pp. 109–115, 2004.

[15] H. H. Wu, A. P. Hu, P. Si, D. Budgett, C. Tung, and S. Malpas, "A push-pull resonant converter with dual coils for transcutaneous energy transfer systems," in *2009 4th IEEE Conference on Industrial Electronics and Applications, ICIEA 2009*, 2009, pp. 1051–1056.